AMERICAN METEOROLOGICAL SOCIETY

Monthly Weather Review

EARLY ONLINE RELEASE

The DOI for this manuscript is doi: 10.1175/MWR-D-14-00034.1

The final published version of this manuscript will replace the preliminary version at the above DOI once it is available.

If you would like to cite this EOR in a separate work, please use the following full citation:

Beavis, N., T. Lang, S. Rutledge, W. Lyons, and S. Cummer, 2014: Regional, Seasonal, and Diurnal Variations of Cloud-to-Ground Lightning with Large Impulse Charge Moment Changes. Mon. Wea. Rev. doi:10.1175/MWR-D-14-00034.1, in press.

Regional, Seasonal, and Diurnal Variations of Cloud-to-Ground Lightning with Large Impulse Charge Moment Changes

Nick K. Beavis

Colorado State University, Fort Collins, CO 80523

Timothy J. Lang

NASA Marshall Spaceflight Center, Huntsville, AL 35812

Steven A. Rutledge (Corresponding Author)

Colorado State University, Fort Collins, CO 80523

rutledge@atmos.colostate.edu

Walter A. Lyons

FMA Research, Inc., Fort Collins, CO 80524

Steven A. Cummer

Duke University, Durham, NC 27705

Submitted to *Monthly Weather Review*

Revised 16 May 2014

Abstract

The use of both total charge moment change (CMC) and impulse charge moment change (iCMC) magnitudes to assess the potential of a cloud-to-ground (CG) lightning stroke to induce a mesospheric sprite has been well described in literature, particularly on a case study basis. In this climatological study, large iCMC discharges for thresholds of > 100 and > 300 C km in both positive and negative polarities are analyzed on a seasonal basis. Also presented are local solar time diurnal distributions in eight different regions covering the lower 48 states as well as the adjacent Atlantic Ocean, including the Gulf Stream.

The seasonal maps show the predisposition of large positive iCMCs to dominate across the Northern Great Plains, with large negative iCMCs favored in the Southeastern U.S. year-round. During summer, the highest frequency of large positive iCMCs across the Upper Midwest aligns closely with the preferred tracks of nocturnal mesoscale convective systems (MCSs). As iCMC values increase above 300 C km, the maximum shifts eastward of the 100 C km maximum in the Central Plains.

Diurnal distributions in the eight regions support these conclusions, with a nocturnal peak in large iCMC discharges in the Northern Great Plains and Great Lakes, an early- to mid-afternoon peak in the Intermountain West and the Southeastern US, and a morning peak in large iCMC discharge activity over the Atlantic Ocean. Large negative iCMCs peak earlier in time than large positive iCMCs, attributed to the growth of large stratiform charge reservoirs following initial convective development.

1. Introduction

Almost a century ago, C.T.R. Wilson predicted atmospheric breakdown high above thunderstorms (Wilson 1925). Remarkably, the topic remained relatively untouched until 1989, with the (re)discovery of sprites - a category of transient luminous events (TLEs) in the mesosphere (Franz et al. 1990). Boccippio et al. (1995) found that sprites were often coincident with highly energetic positive cloud-to-ground (+CG) strokes in the stratiform region of mesoscale convective systems (MCSs) which produced large Schumann resonance excitations detectable in extremely low frequency (ELF) radio waves. Huang et al. (1999) showed that CGs with large charge moment changes (CMCs) were detectable as Q-bursts, which are standouts from background noise embedded in Schumann resonance observations (Ogawa et al. 1966). Since then, measurements of charge moment change, the product of total charge transferred and the vertical lightning channel's length, has been used to infer a sprite's occurrence from a CG (Cummer and Inan 2000). This has in turn revealed much about the tropospheric electrical activity linked to mesospheric sprite production. The total CMC magnitude of a lightning discharge covering the entire duration of a return stroke and continuing current, particularly positive CGs, is strongly linked to the production of sprites (Boccippio et al. 1995, Huang et al. 1999, Pasko et al. 2001, Hu et al. 2002, Cummer and Lyons 2005). However, the availability of total CMC retrievals is limited in large, continental-scale applications because of the laborious manual hand-fitting of waveforms required to produce the CMC for the entire stroke's duration (Lyons and Cummer 2008). The impulse charge moment change (iCMC), representing the charge moment change during the first 2 ms of the stroke (Cummer and Lyons 2004) can effectively measure the charge moment associated with the return stroke and initial continuing current of a lightning discharge (Rakov and Uman 2003). The retrieval of iCMC values can be automated and thus be available at continental scales (Cummer et al. 2013) in real-time (Lyons

78 and Cummer 2008). Moreover, iCMC has been proven to be a highly reliable indicator of the
79 probability of a sprite from a given CG (Lyons and Cummer 2008, Lyons et al. 2009).
80 Recent studies using iCMC retrievals have focused primarily on specific cases. Analysis
81 of a mesoscale convective system (MCS) during the Severe Thunderstorm Electrification and
82 Precipitation Study (STEPS) project (Lyons et al. 2003, Cummer and Lyons 2004) revealed the
83 versatility and importance of iCMC data in that it can be measured remotely for a large amount
84 of strokes in widespread precipitation systems, such as MCSs. Studies such as Cummer and
85 Lyons (2005) further explored iCMC thresholds and the occurrence of sprites over MCSs, which
86 are common over the Great Plains, while more recent studies by Lang et al. (2010, 2011a)
87 analyzed both the iCMC and total CMC of CGs within MCSs, highlighting the significance of
88 continuing current in diagnosing the magnitude and duration of the CMC generally required for
89 the initiation of sprites. The propensity for sprite production above MCSs (Boccippio et al. 1995,
90 Lyons 1996) was reinforced by Sao Sabbas et al. (2010) in a study of a prolific sprite-producing
91 MCS over Argentina, where the bulk of the observed sprites occurred over the stratiform
92 precipitation region. Further studies such as Soula et al. (2009) and Soula et al. (2014) also
93 support the observation of sprites above MCSs. Recently, Cummer et al. (2013) produced
94 density maps, identifying preferential regions for large-iCMC (>100 C km) occurrences across
95 the United States, making use of the utility of near real-time capabilities. These regions
96 somewhat match the regions where warm-season MCSs are common (Fritsch et al. 1986,
97 Carbone et al. 2002). However, no seasonal or diurnal studies of large-iCMC climatologies
98 have been presented to date.
99 Common CG strokes are associated with iCMC values of <50 C km (Cummer and Lyons
100 2004). The theoretical minimum on sprite initiation from total CMC data has been reported to be
101 200 C km (Qin et al 2012), although sprites have been observed from CGs with CMCs as low as
102 120 C km (Hu et al 2002). Thus, the type of lightning analyzed in this study is as Williams et al.
103 (2012) termed as “exceptional” or “superlative” lightning that can loudly “ring” the Earth-

ionosphere cavity as detected by Schumann resonance measurements. Such powerful strokes, and especially those with long continuing currents, are important to many engineering aspects, such as aviation safety and construction. The amount of charge transferred to ground by a CG has until now been routinely estimated. Only the peak current is reported by the NLDN (with no information provided on the continuing current). However, the total charge lowered to ground by a CG can be obtained if a combination of CMC measurements and lightning mapping array (LMA) data is available (Lyons et al. 2003, Lang et al. 2010, Lang et al. 2011b). Since large iCMC strokes have order of magnitude larger iCMCs than garden-variety CGs, then the charge transferred to ground would also be presumed to be at least an order of magnitude larger. Strokes with high charge transfer could be damaging to aircraft and electrical systems, as well as have a higher propensity for triggering fires (e.g. wildfires, structure fires; Curran et al. 2000). Additionally, upward-triggered lightning from tall objects (e.g. towers) has been noted to coincide with large iCMC discharges (Warner 2011, Warner et al. 2012a, 2012b).

. In addition to climatologies of large iCMCs, comparison with NLDN climatologies can reveal the behavior of large-iCMC strokes in relation to CG strokes. Diurnal and seasonal distributions for regions covering the entire contiguous United States as well as national seasonal maps have been prepared, in an effort to better understand the behavior of large iCMCs on long temporal scales. Distributions of iCMCs > 100 C km (similar to Cummer et al. 2013) and larger iCMCs > 300 C km will help to understand the climatology of sprites, as well as their spatial and temporal distribution on a variety of scales.

2. Data

This study utilizes of two main data components: real-time iCMC estimates from the national Charge Moment Change Network (CMCN) as well as flash data from the NLDN.

130 *a. Charge Moment Change Network*

131

132 The CMCN is comprised of two stations: one near Duke University in Durham, NC at
133 35.975°N, 79.100°W and the other at Yucca Ridge Field Station (YRFS), outside Fort Collins,
134 CO at 40.668°N, 104.937°W (Lyons and Cummer 2008, Cummer et al. 2013). The stations
135 measure in the 2 Hz to 25 kHz frequency range (ELF to very low frequency, or VLF; Cummer et
136 al. 2013). The iCMC is diagnosed from ELF magnetic field observations, using linear
137 regularization techniques developed by Cummer and Inan (2000) to extract the charge moment
138 waveform. NLDN flash data are used for geolocation of the iCMC parent stroke and quality
139 control (Cummer and Inan 2000), and thus timing and geolocation uncertainties are tied to the
140 NLDN's uncertainty levels, which are low (Cummins and Murphy 2009). As mentioned by
141 Cummer et al (2013), NLDN-detected events with peak currents less than 10 kA are not
142 processed for iCMCs due to the high number of events of this type. ELF signals from lightning
143 are easily measured over distances longer than 2000 km (Hu et al. 2002, Cummer and Lyons
144 2004), and consequently the two-station CMCN provides measurement coverage over the entire
145 conterminous United States, shown in Fig. 1. In the case of duplicate detections in the
146 overlapping region, the Duke sensor is given preference due to less noise at that sensor (Lyons
147 and Cummer 2008, Cummer et al. 2013). The uncertainty in the iCMC measurements
148 themselves is described in Cummer et al. (2013), who found that two independent
149 measurements of the same stroke resulted in the majority of events having iCMC values that
150 agreed within a factor of 1.5. Consequently, the error bar for the iCMC of an individual event is
151 +50%/-33%. Additional information about the iCMC dataset can be found in Lyons and Cummer
152 (2008) and Cummer et al. (2013). The processed iCMC dataset used by this study extends
153 continuously from 1 August 2007 to 31 July 2012, for 5 complete years of data.

154

155 *b. National Lightning Detection Network*

NLDN flash-level data spanning the same time period were also used in this study. Contained within the NLDN data are geolocation, time, peak current, an intracloud (IC) or CG flag, as well as other parameters such as multiplicity (Cummins et al 1998a). The description and system performance of the NLDN following the installment of a time-of-arrival locating feature is detailed by Cummins et al. (1998a). Recent upgrades included the criteria for classifying positive CG events being any CG-flagged flash with peak current magnitude larger than 15 kA (classifying those below this threshold as ICs; Murphy and Cummins 2009), or an intracloud-identified flash with peak current magnitude larger than 25 kA (K. Cummins 2013, personal communication). If the NLDN fails to detect a CG, then the accompanying iCMC stroke will not be entered into the database. Approximately 10% of sprite-class +CGs are not processed by the NLDN in real-time. Thus, the estimates of the large iCMC population in this study are slightly lower than in reality. These criteria are applied in this study to identify CG flashes in the domains shown in Fig. 1.

3. Methodology

The diurnal and seasonal climatology of large-iCMC and NLDN events focused on regions identified by surface topographical differences as well as lightning differences. Figure 1 shows the selected regional domains. Beginning in the west, the Pacific Coast (PAC) region was meant to capture mostly isolated large-iCMC events associated with cold-season extratropical cyclones making landfall along the U.S. West Coast (Lyons et al 2012; Orville and Huffines 2011) and isolated, primarily terrain-driven warm-season convection. The Intermountain West (MTN) domain was meant to capture most of the Rocky Mountain cordillera along with the isolated, terrain-induced convection common in summer months, often associated with the North American Monsoon (NAM; Badan-Dangon et al. 1991). The western

edge of the MTN region was chosen based on variability studies on the NAM, in which incursions of monsoonal influence can reach southeastern CA and the Great Basin (Barlow et al. 1999, Higgins and Shi 2001), extending northward to separate the wet coastal regime of western Oregon and Washington from the arid regime in eastern Oregon and Washington (Baker 1944). Because the Rocky Mountains curve westward in the northern reaches of the domain, some storms more characteristic of the Northern Great Plains may be captured as well. The southern border of the Northern Great Plains (NGP) domain was placed in the middle of Kansas to capture the observed maximum in positive CG (+CG) percentage extending from western Kansas north-northeastward to southern Manitoba (Lyons et al. 1998, Zajac and Rutledge 2001, Orville et al 2011). The NGP region has also contributed to the bulk of known optical sprite observations (Lyons 1996, Lyons et al. 2003, 2006, 2009). The Great Lakes (LAKE) region was selected to contain the Great Lakes, which can modulate summer convection significantly, including mesoscale squall lines (Lyons 1966, Nicholson and Yin 2002). The Southern Great Plains (SGP) has NGP as a northern boundary, and the eastern boundary for SGP was chosen to exclude the differing topography associated with the Ozark Mountains, which tends to affect overall flash densities (Orville et al. 2011). The Southeastern US (SEUS) was the remainder of the U.S. south and east of the SGP and LAKE regions, containing much of the high-multiplicity -CG lightning observed over the United States (Orville et al 2011). Convection over the Gulf Stream produces enough lightning (Hobbs 1987, Orville 1990) to warrant its own region, and thus the Atlantic Ocean (ATL) domain is meant to contain as much of the Gulf Stream in its domain as possible. The Northeast (NE) domain contains the remainder of the conterminous US for completeness.

Since both iCMC and additional continuing current contribute to the total charge moment change, an iCMC of 100 C km is adjudged to be an adequate lower limit for “large” iCMCs (following Cummer et al. 2013). However, a fixed lower threshold on CMC (and iCMC) is unlikely, but rather a range of CMC over which the probability of sprite initiation increases from

minimal to highly likely (Hu et al. 2002). Lightning events were considered "sprite-class" if their iCMCs were above 300 C km, owing to a 75-80% probability of sprite initiation from a +CG (Cummer and Lyons 2005; Lyons et al. 2009). The 300 C km threshold is also the theoretical minimum threshold for a -CG to produce a sprite (Qin et al. 2012).

Within each region, large iCMC events > 100 C km and sprite-class iCMCs > 300 C km were sorted into hourly (local solar time) bins to produce diurnal distributions. The local solar time for iCMC event can be computed by extracting the observed UTC time from the CMCN and adjusting for the longitude of each observation. The NLDN CG events also were sorted in the same manner in each region.

Hovmoller diagrams of iCMC activity for both large and sprite-class events are also utilized in this study. The spatial domain of these Hovmoller diagrams is the same as in Carbone et al. (2002), with resolution of 1° longitude strips and 1 hour used to produce the time-longitude plots. A very active convective period, 10 June 2011 to 22 June 2011, was chosen to illustrate the progression of large iCMCs with associated convective systems (discussed below).

4. Results

a. National maps of large-iCMC cloud-to-ground lightning

Cummer et al. (2013) presented three-year national stroke density maps for large iCMC ($\geq$100 C km) CG lightning strokes in the United States and surrounding areas. In the present analysis, this has been extended to five years (August 2007 through July 2012). The 5-year stroke density maps (2° latitude/longitude resolution) for iCMC values greater than 100 C km are shown in Fig. 2a and 2b. For the positive (Fig. 2a) strokes (559,562 total for the 5 years), the extended results remain fundamentally similar to the 3-year climatology shown in Cummer et al. (2013; their Fig. 12). The positive maximum remains in central Nebraska, with secondary

maxima centered on western Tennessee (plus portions of surrounding states) and over the Gulf Stream. The positive maximum in the NGP is interesting since this region is well known for its high positive CG percentage (e.g., Orville et al. 2011), as well as for large positive peak currents (Lyons et al. 1998, Orville et al. 2011). While the Gulf Stream is a known lightning hot spot (Christian et al. 2003), Tennessee was not previously known for anomalously powerful +CG lightning using conventional metrics from the NLDN (e.g., Lyons et al. 1998, Orville et al. 2011).

The large positive iCMC maxima are geographically offset from the negative maximum (Fig. 2b; 403,802 strokes total for the 5 years), which occurs over the Gulf Coast (eastern Louisiana through western Florida). This region is known for high flash densities (for both CG and total lightning; Christian et al. 2003, Orville et al. 2011). However, the Gulf Stream remains active for large-iCMC negatives in addition to positives, similar to the peak current results in Lyons et al. (1998). Cummer et al. (2013) did not present a corresponding map for -100 C km strokes.

The 5-year climatologies were broken down by season for positive (Fig. 3) and negative (Fig. 4) strokes with iCMC > 100 C km. In order to improve dynamic range in these plots, the stroke totals have been annualized (i.e., extrapolated to a full year) based on the amounts during each season, and thus densities can be larger than the values shown in Fig. 2. In the winter (Fig. 3a), large positive iCMCs mainly occurred over the southeastern United States . There is another small maximum over the Gulf Stream. Large positive iCMC stroke densities increase and move northward and westward in the spring (Fig. 3b). Gulf Stream activity grows in magnitude and extent during this season. In summer (Fig. 3c), activity again continues its northward and westward march, and there is a very strong maximum over central Nebraska, which is clearly the cause of the same maximum seen in the overall climatology (Fig. 2a). Significant large iCMC activity (at least 10^{-2} km^{-2} yr^{-1} annualized stroke density) reaches its greatest spatial extent during summer, including increased activity in northwestern Mexico, evidently associated with the North American Monsoon (Adams and Comrie 1997). The Gulf

Stream continues to be active as well. Large positive iCMCs decrease rapidly in the fall (Fig. 3d).

In the winter (Fig. 4a), large negative iCMCs are displaced southwestward of the positive maximum, although the negatives remain in the SEUS. This maximum increases in density during the spring (Fig. 4b), while activity also spreads northwestward to form a secondary maximum over Arkansas, and activity over the Gulf Stream develops. Maximum spatial coverage occurs in summer (Fig. 4c), similar to large positive iCMCs (Fig. 3c), but again there is a notable regional offset. Large negative iCMCs continue to dominate in the Southeast, even as the overall activity spreads northwestward into the Central Plains and the desert Southwest/northwestern Mexico. There is a secondary maximum in the Central Plains, but it is displaced eastward from the positive maximum. The Gulf Stream is significantly more active for negatives in summer than spring. Finally, during autumn months, (Fig. 4d) activity declines appreciably

To examine the sensitivity of these large-iCMC climatologies to the choice of threshold, and to look for interesting differences that may reflect the influence of precipitation system evolution, the basic >300 C km climatologies are shown in Fig. 2c and 2d. Despite the approximate factor of 10 reduction in stroke density by moving to the higher threshold (74,585 positive strokes over the 5-year period, and 15,140 negative strokes), the >300 C km climatologies are fundamentally similar to the >100 C km climatologies. One notable difference, however, is that the positive maximum in the Central Plains (Fig. 2c) is displaced slightly eastward of the >100 C km. This was also seen in the 3-year climatology presented in Cummer et al. (2013).

The western Tennessee secondary maximum is not displaced, though, and neither is the negative maximum, which remains over southern Louisiana and Mississippi. Another interesting difference is that the Gulf Stream is a much larger producer of >300 C km positives relative to >300 C km negatives, whereas for >100 C km strokes the production was nearly equal. This

286 may reflect the fact that very few -CGs produce extremely high iCMC values, compared to +CGs
287 (Cummer et al. 2013).
288 The seasonal variability of >300 C km +CGs (Fig. 5) is fundamentally similar to the >100
289 C km +CGs, but the eastward displacement of the >300 C km maximum in the Central Plains
290 (particularly into Iowa) is most prevalent during summer (Fig. 5c). The seasonal variability of
291 >300 C km -CGs (Fig. 6) is very similar to the >100 C km strokes, though again there is a much
292 greater relative reduction for negative strokes at this higher threshold than there is for positive
293 strokes (Cummer et al. 2013).
294 The number of days per grid cell where at least one sprite-class iCMC was observed is
295 presented in Fig. 7. Here, an interesting divergence between positive and negative sprite-class
296 lightning is observed. The frequency for both polarities is highest over the SEUS, as well as the
297 Gulf Stream. While stroke density maxima for sprite-class negatives are observed in the SEUS
298 (Fig. 2d), there is no corresponding frequency maximum in the NGP seen for sprite-class
299 positives (Fig. 7a). This strongly implies that the stroke density maximum observed there (Fig.
300 2c) is almost entirely the result of a very small number of active days over the 5-year period.
301
302 *b. Regional diurnal distributions of large-iCMC CG lightning*
303
304 Figs. 8 and 9 show diurnal distributions for all regions labeled in Fig. 1. Overall, a strong
305 diurnal trend is present in all regions, with large negative iCMCs typically peaking prior to
306 positive iCMCs in afternoon and evening. Sprite-class iCMCs (> 300 C km) are predominantly
307 positive (Table 1). In addition, the 100 C km peak for both polarities occurs earlier than the 300
308 C km peak in all regions. Results from regional diurnal analysis for both thresholds (>100 C km
309 and >300 C km) are summarized below.
310 Evident in nearly every region is an offset in timing between the peak of large iCMC
311 activity and the peak of sprite-class iCMC activity. This offset is most easily visible in the central

US regions (NGP, SGP, SEUS, and LAKE; Figs. 8 and 9c, d, e, and f), where the evening peak in large iCMC activity occurs typically 2-4 hours before the nocturnal peak in sprite-class iCMC activity in those regions. The NGP, SGP, and LAKE regions also shared a tendency for the afternoon and evening large positive iCMC activity to peak before the large negative iCMC activity (Figs. 8 and 9c,d, and e).

The NGP, SGP, and LAKE regions all shared a broad tendency for evening or nocturnal peaks in both large positive and negative iCMC activity, with further nocturnal peaks in sprite-class iCMC activity, predominantly positive across these regions. Despite the tendency of large iCMCs to occur in mid-afternoon in SEUS, the region's sprite-class iCMC behavior was generally similar to the NGP, SGP, and LAKE regions, with a nocturnal peak in both polarities.

Large iCMC tendency in the MTN region (Fig. 8b) was much different than the other seven regions, save for SEUS, with virtually no iCMC activity occurring from 0000-0900 LST. A sharply-defined peak in large iCMC activity of both polarities occurs in mid-afternoon, around 1300-1400 LST for negatives and 1500-1600 LST for positives. The sprite-class iCMC behavior in MTN resembles the large iCMC behavior, with the peak in sprite-class negative iCMCs occurring nearly concurrently with the peak in large negative iCMCs around 1300-1400 LST (Fig. 9b). The sprite-class positives are shifted later in time, much more like the other continental regions, but the peak remains much narrower temporally. The peak in large iCMC activity in SEUS, most notably large negative iCMC activity, occurs around 1500 LST (Fig. 8f). However, the large positive iCMC activity in SEUS (Fig. 8f) more closely resembles large positive iCMC activity in NGP, SGP, and LAKE, with a nocturnal peak at approximately 1900 LST.

Oceanic ATL observations present a shift from the predominantly land-based domains. Large iCMCs >100 C km (Fig. 8h) show a broad morning peak from 0300 to 0700 LST, while sprite-class iCMCs displayed a mid-morning peak broadly extending from 0600 to 1200 LST. Also of note are the low iCMC counts in the PAC and NE regions (Table 1). The irregular

diurnal behavior seen especially in these regions (Figs. 8a, 8g, 9a, and 9g) is due to the lack of lightning activity.

Overall, the NLDN CG observations show a strong diurnal signal, with most continental regions peaking in CG activity by 1600 LST. The NLDN activity peaks occur before the maxima in total iCMC activity in all regions. In general, there is a much greater possibility for a +CG to have a large or sprite-class iCMC compared to a -CG in all regions (Fig. 10). The NGP region has a relatively higher ratio of large iCMCs to all CGs, especially in positives. Also seen in Fig. 10, the percentages of sprite-class iCMCs to large iCMCs are much higher for positive strokes than negative strokes.

c. Hovmoller diagrams of large and sprite-class iCMC events

Fig. 11 illustrates the time-longitude behavior of iCMC events larger than 100 C km (Fig. 11a) and 300 C km (Fig. 11b). Noticeable during the selected active convective period are both an eastward displacement in longitude and a lag in time of the > 300 C km event maxima from the >100 C km event maxima. This observation is illustrated in Fig. 11b, where the maxima from the 100 C km plot (white vertical lines) are displaced westward and earlier in time than the 300 C km maxima (black vertical lines). Implied phase speeds from these active periods are varied, but average 15 ms^{-1}, consistent with phase speed observations of mesoscale systems presented in Carbone et al. (2002) of 14-18 m s^{-1}. Estimated phase speeds are not appreciably different between 100 C km and 300 C km data. Also seen in the iCMC data are coherent systems propagating across the United States, most notably seen from late 19 June 2011 through 21 June 2011. This observation of coherent patterns in the iCMC data matches observations in Carbone et al. (2002) of coherent rainfall patterns.

5. Discussion and Conclusions

The presence of a broad maximum in large positive iCMCs in the Central Plains (e.g., Nebraska) is notable, as this region is well known to be associated with broad maxima in mesoscale convective complexes (MCCs; Maddox 1980), including track locations, the fraction of annual and warm-season precipitation produced by (often nocturnal) MCCs, as well as cold cloud top frequency (Fritsch et al. 1986, McAnelly and Cotton 1989, Ashley et al. 2003). This region also is well known to contain broad maxima in +CG percentage, peak current, and multiplicity along with broad minima in the corresponding -CG characteristics (Lyons et al. 1998, Orville and Huffines 2001, Zajac and Rutledge 2001, Rudlosky and Fuelberg 2010, Orville et al. 2011). Additionally, this region contains a relative maximum in IC-to-CG lightning ratio (Boccippio et al. 2001). Many studies also have documented the northwestward march of MCC tracks (Velasco and Fritsch 1987, Augustine and Howard 1991, Ashley et al. 2003), CGs (Holle et al. 2011), and total lightning (Christian et al. 2003) from the southeastern United States into the Central Plains as seasons transition from winter to spring to summer. This behavior is also observed in the large-iCMC lightning data for both polarities.

It is therefore reasonable to infer that MCCs and MCSs, with their ability to produce high lightning flash rates (Goodman and MacGorman 1986, Carey et al. 2005, Lang and Rutledge 2008, Makowski et al. 2013), and an enhanced percentage of +CG lightning in their stratiform regions (Orville et al. 1988, Rutledge and MacGorman 1988, Rutledge et al. 1990, MacGorman and Morgenstern 1998), play a significant role in the presence of many of these regional features. Given the known link between MCSs and the production of sprites (Boccippio et al. 1995, Lyons 1996, 2006, Lyons et al. 2003, Williams and Yair 2006, Lang et al. 2010), and the known link between sprite occurrence and large-CMC discharges (Wilson 1925, Boccippio et al. 1995, Huang et al. 1999, Hu et al. 2002, Cummer and Lyons 2005, Lyons et al. 2009, Lang et al. 2011a, Qin et al. 2012), the approximate collocation of the large iCMC positive maximum with

389 other lightning- and storm-related maxima in the Central Plains (NGP, SGP, LAKE) is thus
390 expected.

391 The present study supports the conclusions of Cummer et al. (2013) that a slight
392 eastward bias exists for stroke density of +CGs with > 300 C km when compared to ones with >
393 100 C km, particularly for the Central Plains. This is consistent with the composite-MCC life
394 cycle study of McAnelly and Cotton (1989), which found that MCCs on average grow in size and
395 reach full maturity eastward of central Nebraska. The nocturnal peak in large positive iCMCs is
396 also most clearly associated with upscale development of MCSs (McAnelly and Cotton 1989).
397 Larger (sprite-class) iCMCs are favored nocturnally as MCS stratiform regions develop and
398 expand during this time period, allowing for a larger positive charge reservoir in the stratiform
399 region (Boccippio et al. 1995, Williams 1998, Lyons 1996, 2006, Lyons et al. 2003, Williams and
400 Yair 2006, Lang et al. 2010, Soula et al. 2009, 2014), and a greater frequency of larger iCMC
401 positives would be expected (Cummer et al. 2013). The tendency of a larger percentage of
402 positive CGs in the NGP than in other regions to be large or sprite-class (Figs. 10a, 10b) also
403 supports this conclusion. Regionally, the LAKE region's more nocturnal peak in iCMC activity
404 than NGP can be attributed to MCS advection from the NGP region (McAnelly and Cotton 1989).
405 The distinct shift of the >300 C km iCMC maximum southeastward of the maximum in overall
406 CG activity and >100 C km iCMC activity (Boccippio et al. 2001, Orville et al. 2011) is also well
407 attributed to the advection and maturation of MCSs and their associated stratiform charge
408 reservoirs.

409 Fig. 11 readily supports speculation of the association of large and sprite-class iCMCs to
410 MCSs, especially in the Great Plains. Average observed phase speeds of 15 m s^{-1} shown by the
411 large-iCMC data match observed phase speeds of 14-18 m s^{-1} of mesoscale systems identified
412 in Carbone et al. (2002) across the longitudes of the Great Plains and this study's NGP region.
413 Additionally, the systems producing sprite-class iCMCs in Fig. 11b are presumably more mature
414 systems that have moved to the east over their lifetimes than the systems producing large

iCMCs in Fig. 11a. Additionally, Figs. 11a and 11b show that across the longitudes of the Great Plains in this warm-season period, large and sprite-class iCMCs are almost exclusively produced by systems with lifetimes and propagation speeds befitting of MCSs. Thus, a strong association of large and sprite-class iCMCs to MCSs especially in the warm season is reasonable, with a stronger likelihood of production of sprite-class iCMCs as the systems mature and propagate eastward.

Two other secondary maxima in both polarities of large-iCMC lightning are notable, and both further solidify the inferred association between large-iCMC lightning and mesoscale precipitation systems. One is the increase in stroke density during summer over the southwestern United States and northwestern Mexico (MTN). As stated previously, this region is strongly affected by the North American Monsoon (Adams and Comrie 1997), and mesoscale systems produce a large fraction of the seasonal rainfall (Lang et al. 2007), much like the Central Plains. Convective development by strong daytime forcing is evident especially in the MTN region. Based on the observations, large negative iCMCs may be generally associated with areas of convective development, consistent with Lang et al. (2013). However, as storms mature and produce large anvils, some possibly interacting with each other, stratiform charge reservoirs similar to those in MCSs can develop, and extending the conclusions from Orville et al. (1988), Rutledge and MacGorman (1988), Rutledge et al. (1990), and MacGorman and Morgenstern (1998), the enhanced large positive iCMC signal in MTN suggests that the increased +CG activity associated with increased stratiform area becomes evident, perhaps also in part due to the end-of-storm oscillation process (Williams 1998, Pawar and Kumra 2007).

Additionally, the Gulf Stream (ATL) is associated with rainfall and lightning enhancement year round (Christian et al. 2003, Virts et al. 2013), in part due to increased cyclogenesis and the anchoring of large precipitation systems over the warm ocean current (Minobe et al. 2008) as well as winter monsoon cold air advection (Price and King 2002). Diurnally, the ATL region shows a typical oceanic distribution of convection, with a morning maximum in iCMCs > 100 C

441 km as well as CGs roughly coinciding with maxima in oceanic convection and precipitation found
442 in oceanic MCSs and deep convective cores by Romatschke et al. (2010) to be around 0500-
443 0800 local time. Liu and Zipser (2008) as well as Romatschke et al. (2010) noted broad
444 stratiform coverage over oceanic regions by midday, consistent with the maximum in sprite-
445 class positive iCMCs over the ATL region near local midday. This also supports speculation
446 concerning the occurrence of sprites over the Gulf Stream (Price and King 2002).

447 The NE and PAC regions show very little iCMC activity compared to the other regions
448 (Table 1). The PAC region is heavily positive iCMC-dominated; the amount of large iCMCs was
449 so low that they appeared to be mostly isolated in nature, possibly associated with stratiform
450 regions within extratropical cyclones making landfall on the Pacific Coast, especially in winter
451 (Lang et al. 2011b, Lyons et al. 2012). In the SGP, SEUS, and LAKE regions, a noticeable peak
452 in negative iCMC activity was observed as overall activity began to decline near 0400 LST,
453 nearing dawn. All of these regions are predominantly land, but contain some portion of ocean or
454 very large bodies of water (Fig. 1), so a small modulation by oceanic diurnal convective
455 tendencies (Liu and Zipser 2008, Romatschke et al. 2010) may be the explanation of these
456 upticks in negative (and in some cases positive) iCMC activity, most notably the SEUS region.

457 What remains difficult to explain is the regional offset between large negative iCMCs
458 (dominating in the southeastern United States) and large positive iCMCs (dominating in the
459 Central Plains), which is especially present during the summer months (June-August). A
460 potential clue for why this occurs may be found in the sprite-class frequency plot (Fig. 7), which
461 strongly supports the inference that a very small number of storm days contributes to the NGP
462 positive maximum, unlike other regions. Examining the clearly exceptional nature of NGP
463 storms on these sprite-class days is planned for a future study.

464 The regional offset is not as pronounced during other seasons. For example, maxima in
465 large-iCMC lightning of either polarity exist near the Kansas/Missouri border region during the
466 fall. Also, such an offset is not seen over the Gulf Stream or in the North American Monsoon

region. Moreover, large positive iCMCs are common in the Southeast during the winter months, when the main tracks of MCSs remain south of the Central Plains (e.g., Velasco and Fritsch 1987). Additionally, the occurrence of large iCMCs in these cold-season MCSs and in frontal systems with very large stratiform cloud shields has not been explored extensively.

Assuming this holds true for the broader population of strokes in this study, then the results would be consistent with convection situated mostly eastward of stratiform precipitation in the Central Plains (i.e., a preference for eastward-moving leading-line, trailing stratiform MCSs during summer; Parker and Johnson 2000), while southeastern precipitation systems may not feature pronounced stratiform regions during summer, perhaps due to the influence of the sea-breeze in organizing convection along the Gulf Coast and weak tropospheric wind shear. For example, Lang et al. (2013) presented an example of a prolific large-iCMC -CG producing storm that was oriented parallel to the coast with no well-developed stratiform precipitation.

Diurnal curves of CGs match the findings of the NLDN diurnal distributions by Holle (2013), with a good agreement temporally on the peak of total CG activity in each region. The peaks in CG activity (Figs. 8 and 9), especially the nocturnal predisposition in the Northern Great Plains and mid-afternoon peaks over the Rockies and Southeastern US, are also supported by Holle (2013). The total CG peak still occurs well before the iCMC peak temporally, with the majority of large-iCMC discharges coming while the CG peak is in its decline. This tendency of iCMCs to follow the CGs in time is especially evident in the MTN region.

Clearly, these somewhat speculative hypotheses require further refinement and testing, in particular utilizing data from the national network of radars in the United States. The meteorology of systems producing large-iCMC lightning can further support the development of conclusions regarding large-iCMC production, most notably the link between stratiform charge reservoirs in MCSs as well as the association of large negative iCMCs with areas of convection. The size of the system may be important for whether it produces more or greater magnitude

493 iCMC discharges than smaller systems, and may affect preferred polarities. Analysis of
494 individual iCMC-producing storms is currently underway.
495
496 ## Acknowledgements
497 The authors gratefully acknowledge the support of Vaisala, Inc. in providing the National
498 Lightning Detection Network Data on which the CMCN is built as well as the support of the
499 Missile Defense Agency SBIR Program. The National Science Foundation provided support for
500 this work under Grant AGS-1010657, and DARPA provided additional funding support under the
501 Nimbus program. The authors also would like to extend thanks to the Radar Meteorology Group
502 at Colorado State University for valuable scientific input, and especially Paul Hein for invaluable
503 computing support. Thanks also to Prof. Russ Schumacher and four anonymous reviewers for
504 insightful scientific input and suggestions. The views, opinions, and findings in this report are
505 those of the authors, and should not be construed as an official NASA or U.S. Government
506 position, policy, or decision.
507

References

Adams, D. K. and A. C. Comrie, 1997: The North American Monsoon. *Bull. Amer. Meteor. Soc.*, **78**, 2197-2213.

Augustine, J. A. and K. W. Howard, 1991: Mesoscale Convective Complexes over the United States during 1986 and 1987. *Mon. Wea. Rev.*, **119**, 1575-1589.

Ashley, W. S., T. L. Mote, P. G. Dixon, S. L. Trotter, E. J. Powell, J. D. Durkee, A. J. Grundstein, 2003: Distribution of Mesoscale Convective Complex Rainfall in the United States. *Mon. Wea. Rev.,* **131**, 3003-3017.

Badan-Dangon, A., C.E. Dorman, M.A. Merrifield, and C.D. Winant, 1991: The Lower Atmosphere over the Gulf of California. *J. Geophys. Res.*, **96**(C9), 16877-16896.

Baker, F. S., 1944: Mountain climates of the western United States. *Ecological Monographs*, **14**(2), 223-254.

Barlow, M., S. Nigam, and E.H. Berbery, 1998: Evolution of the North American Monsoon System. *J. Climate*, **11** (9), 2238-2257.

Boccippio, D.J., E.R. Williams, S.J. Heckman, W.A. Lyons, I.T. Baker, and R. Boldi, 1995: Sprites, ELF transients, and positive ground strokes. *Science*, **269**(5227), 1088-1091.

Boccippio, D.J., K. L. Cummins, H. J. Christian, and S. J. Goodman, 2001: Combined Satellite- and Surface-Based Estimation of the Intracloud-Cloud-to-Ground Lightning Ratio over the Continental United States. *Mon. Wea. Rev.*, **129**, 108-122.

Carbone, R.E., J.D. Tuttle, D.A. Ahijevych, and S.B. Trier, 2002: Inferences of Predictability Associated with Warm Season Precipitation. *J. Atmos. Sci.,* **59**(13), 2033-2056.

Carey, L. D., M. J. Murphy, T. L. McCormick, and N. W. S. Demetriades, 2005: Lightning location relative to storm structure in a leading-line, trailing-stratiform mesoscale convective system. *J. Geophys. Res.*, **110**, D03105, doi:10.1029/2003JD004371.

532 Christian, H. J. et al., 2003: Global frequency and distribution of lightning as observed from
533 space by the Optical Transient Detector. *J. Geophys. Res.*, **108**(D1), 4005,
534 doi:10.1029/2002JD002347.
535 Cummer, S. A. and U.S. Inan, 2000: Modeling ELF radio atmospheric propagation and
536 extracting lightning currents from ELF observations. *Radio Science*, **35**(2), 385-394.
537 Cummer, S.A. and W.A. Lyons, 2004: Lightning charge moment changes in US High Plains
538 thunderstorms. *Geophys. Res. Lett.,* **31**(5), L05114.
539 Cummer, S.A., and W.A. Lyons, 2005: Implications of lightning charge moment changes for
540 sprite initiation. *J. Geophys. Res.*, **110**(A04304), doi:10.1029/2004JA010812.
541 Cummer, S.A., W.A. Lyons, and M.A. Stanley, 2013: Three Years of Lightning Impulse Charge
542 Moment Change Measurements in the United States. *J. Geophys. Res.*,**118**, 5176-5189,
543 doi:10.1002/jgrd.50442.
544 Cummins, K.L. and M.J. Murphy, 2009: An Overview of Lightning Locating Systems: History,
545 Techniques, and Data Uses, with an In-Depth Look at the U.S. NLDN. *IEEE Trans. Elec.*
546 *Comp.*, **51**(3), 499-518.
547 Cummins, K.L., M.J. Murphy, E.A. Bardo, W.L. Hiscox, R.B. Pyle, and A.E. Pifer, 1998a: A
548 Combined TOA/MDF Technology Upgrade of the U.S. National Lightning Detection
549 Network. *J. Geophys. Res.*, **103**(D8), 9035-9044.
550 Curran, E.B., R.L. Holle, and R.E. Lopez, 2000: Lightning Casualties and Damages in the
551 United States from 1959 to 1994. *J. Climate*, **13**, 3448-3464.
552 Franz, R.C., R.J. Nemzek, and J.R. Winckler, 1990: Television image of a large upward
553 electrical discharge above a thunderstorm system. *Science*, **249**(4964), 48-51.
554 Fritsch, J.M., R.J. Kane, and C.R. Chelius, 1986: The Contribution of Mesoscale Convective
555 Weather Systems to the Warm-Season Precipitation in the United States. *J. Climate &*
556 *App. Met.,* **25**(10), 1333-1345.

557 Goodman, S. J., D. R. MacGorman, 1986: Cloud-to-Ground Lightning Activity in Mesoscale
558 Convective Complexes. *Mon. Wea. Rev.*, **114**, 2320-2328.
559 Higgins, R.W., and W. Shi, 2001: Intercomparison of the Principal Modes of Interannual and
560 Intraseasonal Variability of the North American Monsoon System, *J. Climate*, **14**, 403-
561 417.
562 Hobbs, P.V., 1987: The Gulf Stream Rainband. *Geophys. Res. Lett.*, **14**(11), 1142-1145.
563 Holle, R. L., K. L. Cummins, and N. W.S. Demetriades, 2011: Monthly distributions of NLDN and
564 GLD360 cloud-to-ground lightning. *5th Conf. on the Meteorological Applications of*
565 *Lightning Data*, American Meteorological Society, Seattle, WA.
566 https://ams.confex.com/ams/91Annual/webprogram/5LIGHTNING.html.
567 Holle, R.L., 2013: Diurnal Variations of NLDN Cloud-to-Ground Lightning in the United States.
568 *6th Conf. on the Meteorological Applications of Lightning Data,* American Meteorological
569 Society, Austin, TX.
570 Hu, W., S.A. Cummer, W. A. Lyons, and T.E. Nelson, 2002: Lightning charge moment changes
571 for the initiation of sprites. *Geophys. Res. Lett.*, **29**(8), 1279,
572 doi:10.1029/2001GL014593.
573 Huang, E., E. Williams, R. Boldi, S. Heckman, W. Lyons, M. Taylor, T. Nelson, and C. Wong,
574 1999: Criteria for sprites and elves based on Schumann resonance observations. *J.*
575 *Geophys. Res.*, **104**(D14), 16943-16964.
576 Lang, T. J., D. A. Ahijevych, S. W. Nesbitt, R. E. Carbone, S. A. Rutledge, R. Cifelli, 2007:
577 Radar-observed characteristics of precipitating systems during NAME 2004. *J. Climate*,
578 **20**, 1713–1733.
579 Lang, T. J., and S. A. Rutledge, 2008: Kinematic, microphysical, and electrical aspects of an
580 asymmetric bow-echo mesoscale convective system observed during STEPS 2000. *J.*
581 *Geophys. Res.,* **113**, D08213, doi:10.1029/2006JD007709.

582 Lang, T. J., W. A. Lyons, S. A. Rutledge, J. Meyer, D. R. MacGorman, and S. A. Cummer,
583 2010b: Transient luminous events above two mesoscale convective systems: Storm
584 structure and evolution. *J. Geophys. Res.*, **115**, A00E22, doi:10.1029/2009JA014500.
585 Lang, T. J., J. Li, W. A. Lyons, S. A. Cummer, S. A. Rutledge, and D. R. MacGorman, 2011a:
586 Transient luminous events above two mesoscale convective systems: Charge moment
587 change analysis. *J. Geophys. Res.*, **116**, A10306, doi:10.1029/2011JA016758.
588 Lang, T. J., W. A. Lyons, S. A. Cummer, S. Rutledge, and T. E. Nelson, 2011b: Toward a
589 climatology of precipitating systems that produce lightning with large impulse charge
590 moment changes. *5th Conf. on the Meteorol. Appl. of Lightning Data*, *Seattle*, WA, Amer.
591 Meteor. Soc., 4.3,
592 https://ams.confex.com/ams/91Annual/webprogram/Paper184639.html.
593 Lang, T. J., S. A. Cummer, S. A. Rutledge, and W. A. Lyons, 2013: The meteorology of negative
594 cloud-to-ground lightning strokes with large charge moment changes: Implications for
595 negative sprites. *J. Geophys. Res. Atmos,* **118**, doi:10.1002/jgrd.50595.
596 Liu, C. and E.J. Zipser, 2008: Diurnal cycles of precipitation, clouds, and lightning in the tropics
597 from 9 years of TRMM observations. *Geophys. Res. Lett.*, **35**, L04819,
598 doi:10.1029/2007GL0320437.
599 Lyons, W.A., 1966: Some effects of Lake Michigan on squall lines and summertime convection,
600 Proceedings of the 9th Conf. Great lakes Res., University of Michigan, Ann Arbor, MI,
601 259-273.
602 Lyons, W. A., 1996: Sprite observations above the U.S. High Plains in relation to their parent
603 thunderstorm systems. *J. Geophys. Res.*, **101**, 29,641-29,652.
604 Lyons, W. A., M. Uliasz, and T.E. Nelson, 1998: Large Peak Current Cloud-to-Ground Lightning
605 Flashes during the Summer Months in the Contiguous United States. *Mon. Wea. Rev.*,
606 **126**, 2217-2233.

Lyons, W. A., T. E. Nelson, E. R. Williams, S. A. Cummer, and M. A. Stanley, 2003: Characteristics of sprite-producing positive cloud-to-ground lightning during the 19 July 2000 STEPS mesoscale convective systems. *Mon. Wea. Rev.,* **131**, 2417-2427.

Lyons, W. A., 2006: The meteorology of transient luminous events – An introduction and overview. *NATO Advanced Study Institute on Sprites, Elves and Intense Lightning Discharges*, M. Fullekrug et al. (eds.), Springer, 19-56.

Lyons, W.A. and S.A. Cummer, 2008: Stratospheric Lightning: Forecasting and Nowcasting Tools. Final Report, SBIR Phase II, Missile Defense Agency, Contract HQ0006-06-C-7313, FMA Research, Inc., Fort Collins, CO, 298 pp.

Lyons, W. A., M. Stanley, J. D. Meyer, T. E. Nelson, S. A. Rutledge, T. J. Lang, and S. A. Cummer, 2009: The meteorological and electrical structure of TLE-producing convective storms. In Lightning: Principles, Instruments and Applications, H.D. Betz et al. (eds.), 389-417 pp., Springer Science+Business Media B.V., DOI: 10.1007/978-1-4020-9079-0_17.

Lyons, W.A., T.A. Warner, S.A. Cummer, S.A. Rutledge, T.J. Lang, T.C. Meyer, G. Lu, T.E. Nelson, and T. Samaras, 2012: Different Strokes: Researching the Unusual Lightning Discharges Associated with Sprites and Jets and Atypical Meteorological Regimes. Proceedings of the 22nd International Lightning Detection Conference, Boulder, Colorado, 1-4 April 2012, 19 pp.

MacGorman, D. R., and C. D. Morgenstern, 1998:, Some characteristics of cloud-to-ground lightning in mesoscale convective systems. *J. Geophys. Res.*, **103**(D12), 14011-14023, doi:10.1029/97JD03221.

Maddox, R. A., 1980: Mesoscale Convective Complexes. *Bull. Amer. Meteor. Soc.*, **61**, 1374-1387.

631 Makowski, J. A., D. R. MacGorman, M. I. Biggerstaff, and W. H. Beasley, 2013: Total Lightning
632 Characteristics Relative to Radar and Satellite Observations of Oklahoma Mesoscale
633 Convective Systems. *Mon. Wea. Rev.*, **141**, 1593–1611.
634 McAnelly, R. L. and W. R. Cotton, 1989: The Precipitation Life Cycle of Mesoscale Convective
635 Complexes over the Central United States. *Mon. Wea. Rev.*, **117**, 784–808.
636 Minobe, S., A. Kuwano-Yoshida, N. Komori, S.P. Xie, & R.J. Small, 2008: Influence of the Gulf
637 Stream on the Troposphere. *Nature*, **452**(7184), 206-209.
638 Nicholson, S.E. and X. Yin, 2002: Mesoscale patterns of rainfall, cloudiness, and evaporation
639 over the Great Lakes of East Africa. *The East African Great Lakes: Limnology,*
640 *Palaeolimnology, and Biodiversity,* **12**, 93-119.
641 Ogawa, T., Y. Tanka, T. Miura, and M. Yasuhara, 1966: Observations of natural ELF
642 electromagnetic noises by using the ball antennas. *J. Geomagn. Geoelectr.*, **18**, 443-
643 454.
644 Orville, R. E., R.W. Henderson, and L.F. Bosart, 1988: Bipole patterns revealed by lightning
645 locations in mesoscale storm systems. *Geophys. Res. Lett.*, **15**(2), 129-132.
646 Orville, R.E., 1990: Winter Lightning Along the East Coast. *Geophys. Res. Lett.*, **17**(6), 713-715.
647 Orville, R. E. and G. R. Huffines, 2001: Cloud-to-Ground Lightning in the United States: NLDN
648 Results in the First Decade, 1989–98. *Mon. Wea. Rev.*, **129**, 1179–1193.
649 Orville, R.E., G.R. Huffines, W.R. Burrows, and K.L. Cummins, 2011: The North American
650 Lightning Detection Network (NALDN)- Analysis of Flash Data: 2001-09. *Mon. Wea.*
651 *Rev.*, **139**(5), 1305–1321.
652 Parker, M. D. and R. H. Johnson, 2000: Organizational Modes of Midlatitude Mesoscale
653 Convective Systems. *Mon. Wea. Rev.*, **128**, 3413–3436.
654 Pasko, V.P., U.S. Inan, and T.F. Bell, 2001: Mesosphere-troposphere coupling due to sprites,
655 *Geophys. Res. Lett.*, **28**(19), 3821-3824.

656 Pawar, S.D. and A.K. Kamra, 2007: End-of-storm oscillation in tropical air mass thunderstorms.
657 *J. Geophys. Res.*, **112**, D03204, doi:10.1029/2005/JD006997.
658 Price, C., W. Burrows, P. King, 2002: The likelihood of winter sprites over the Gulf Stream.
659 *Geophys. Res. Lett.*, **29**, doi:10.1029/2002GL015571.
660 Qin, J., S. J. Celestin, and V. P. Pasko, 2012: Minimum charge moment change in positive and
661 negative cloud to ground lightning discharges producing sprites. *Geophys. Res. Lett*, **39**,
662 L22801, doi:10.1029/2012GL053951.
663 Rakov, V.A. and M. A. Uman, 2003: *Lightning*. Cambridge University Press, Cambridge, 687 pp.
664 Romatschke, U., S. Medina, and R.A. Houze, 2010: Regional, Seasonal, and Diurnal Variations
665 of Extreme Convection in the South Asian Region. *J. Climate*, **23**, 419-439.
666 Rudlosky, S. D. and H. E. Fuelberg, 2010: Pre- and Postupgrade Distributions of NLDN
667 Reported Cloud-to-Ground Lightning Characteristics in the Contiguous United States.
668 *Mon. Wea. Rev.*, **138**, 3623–3633.
669 Rutledge, S. A., C. Lu, and D. R. MacGorman, 1990: Positive Cloud-to-Ground Lightning in
670 Mesoscale Convective Systems. *J. Atmos. Sci.*, **47**, 2085–2100.
671 Rutledge, S. A., D. R. MacGorman, 1988: Cloud-to-Ground Lightning Activity in the 10–11 June
672 1985 Mesoscale Convective System Observed during the Oklahoma–Kansas PRE-
673 STORM Project. *Mon. Wea. Rev.*, **116**, 1393–1408.
674 Sao Sabbas, F. T. et al., 2010: Observations of prolific transient luminous event production
675 above a mesoscale convective system in Argentina during the Sprite2006 Campaign in
676 Brazil. *J. Geophys. Res.*, **115**, A00E58, doi:10.1029/2009JA014857.
677 S. Soula, O. van der Velde, J. Montanyà, T. Neubert, O. Chanrion, and M. Ganot, 2009:
678 Analysis of thunderstorm and lightning activity associated with sprites observed during
679 the EuroSprite campaigns: two case studies. *Atmos. Res.*, **91**,
680 http://dx.doi.org/10.1016/j.atmosres.2008.06.017

681 S. Soula, F. Iacovella, O. van der Velde, J. Montanyà, M. Füllekrug, T. Farges, J. Bór, J. F.
682 Georgis, S. NaitAmor, J.M. Martin, 2014: Multi-instrumental analysis of large sprite
683 events and their producing storm in southern France. *Atmos. Res*, **135-136**,
684 http://dx.doi.org/10.1016/j.atmosres.2012.10.004.
685 Velasco, I., and J. M. Fritsch, 1987: Mesoscale convective complexes in the Americas. *J.*
686 *Geophys. Res.*, **92**(D8), 9591-9613, doi:10.1029/JD092iD08p09591.
687 Virts, K. S., J. M. Wallace, M. L. Hutchins, and R. H. Holzworth, 2013: Highlights of a new
688 ground-based, hourly global lightning climatology. *Bull. Amer. Meteorol. Soc.*, In Press,
689 doi: http://dx.doi.org/10.1175/BAMS-D-12-00082.1.
690 Warner, T.A., 2011: Observations of simultaneous upward lightning leaders from multiple tall
691 structures. *Atmos. Res.*, 2011, doi: 10.1016/j.atmosres.2011.07.004.
692 Warner, T. A., K. L. Cummins, and R. E. Orville, 2012a: Upward lightning observations from
693 towers in Rapid City, South Dakota and comparison with National Lightning Detection
694 Network data, 2004-2010. *J. Geophys. Res.: Atmos.*, **117**, D19109,
695 doi:10.1029/2012JD018346.
696 Warner, T.A., M.M.F. Saba, S. Ridge, M. Bunkers, W. Lyons and R.E. Orville, 2012b: Lightning-
697 triggered upward lightning from towers in Rapid City, South Dakota. Proceedings, ILDC,
698 Boulder, CO, 9 pp.
699 Williams, E.R., 1988: The positive charge reservoir for sprite-producing lightning, *J. Atmos.*
700 *Solar-Terres. Phys.*, **60**, 689-692.
701 Williams, E. R., V. Mushtak, D. Rosenfeld, S. Goodman, and D. Boccippio, 2005:
702 Thermodynamic conditions favorable to superlative thunderstorm updraft, mixed phase
703 microphysics and lightning flash rate. *Atmos. Res.*, **76**, 288– 306.
704 Williams, E.R. and Y. Yair, 2006: The microphysical and electrical properties of sprite-producing
705 thunderstorms. NATO Advanced Study Institute on Sprites, Elves and Intense Lightning
706 Discharges, M. Fullekrug et al. (eds.), Springer, 57-83.

Williams, E., et al., 2012: Resolution of the sprite polarity paradox: The role of halos. *Radio Sci.*, **47**, RS2002, doi:10.1029/2011RS004794.

Wilson, C.T.R., 1925: The electric field of a thunderstorm and some of its effects. *Proc. Phys. Soc. Lond*, **37**, 32D-37D.

Zajac, B. A. and S. A. Rutledge, 2001: Cloud-to-Ground Lightning Activity in the Contiguous United States from 1995 to 1999. *Mon. Wea. Rev.*, **129**, 999–1019.

Table Captions

Table 1. Tabulation of total iCMC and NLDN CG statistics in each region for the time period August 2007-July 2012.

Figure Captions

Figure 1. Regional domains used in the analysis of iCMC and NLDN diurnal and seasonal climatologies. The short descriptors are as follows: Southern Great Plains (SGP), Northern Great Plains (NGP), Southeastern US (SEUS), Great Lakes (LAKE), New England (NE), Atlantic Ocean (ATL), Intermountain West (MTN), and Pacific Coast (PAC). Also shown on the map is the coverage of the CMCN (dashed black line) as well as the location of the CMCN sensors at YRFS and DU (black dots).

Figure 2. Density maps for strokes with iCMC values greater than 100 C km, for August 2007 through July 2012. (a) Positive strokes. (b) Negative strokes; Density maps for strokes with iCMC values greater than 300 C km, for August 2007 through July 2012. (c) Positive strokes. (d) Negative strokes. Note that the two bottom panels for the >300 C km maps are multiplied by 0.1 of the scale for >100 C km strokes.

Figure 3. Annualized density maps for positive strokes with iCMC values greater than 100 C km, broken down by season for the period August 2007 through July 2012. (a) December through February (Winter). (b) March through May (Spring). (c) June through August (Summer). (d) September through November (Fall).

Figure 4. Annualized density maps for negative strokes with iCMC values less than -100 C km, broken down by season for the period August 2007 through July 2012. (a) December through

February (Winter). (b) March through May (Spring). (c) June through August (Summer). (d) September through November (Fall).

Figure 5. Annualized density maps for positive strokes with iCMC values greater than 300 C km, broken down by season for the period August 2007 through July 2012. (a) December through February (Winter). (b) March through May(Spring). (c) June through August (Summer). (d) September through November (Fall).

Figure 6. Annualized density maps for negative strokes with iCMC values less than -300 C km, broken down by season for the period August 2007 through July 2012. (a) December through February (Winter). (b) March through May (Spring). (c) June through August (Summer). (d) September through November (Fall).

Figure 7. (a) Annual number of days per grid cell with at least one positive sprite-class lightning (iCMC > 300 C km). (b) Annual number of days per grid cell with at least one negative sprite-class lightning (iCMC < -300 C km).

Figure 8. Diurnal distributions of regional iCMC events greater than 100 C km, for the period August 2007- July 2012. (a) Pacific Coast (PAC). (b) Intermountain West (MTN). (c) Northern Great Plains (NGP). (d) Great Lakes (LAKE). (e) Southern Great Plains (SGP). (f) Southeastern United States (SEUS). (g) New England (NE). (h) Atlantic Ocean (ATL).

Figure 9. Same as in Fig. 7, but for iCMC events greater than 300 C km.

764 **Figure 10.** Ratios of (a) total large iCMC (>100 C km) activity to total NLDN CG activity, (b) total
765 sprite-class (>300 C km) iCMC activity to total NLDN CG activity, (c) total sprite-class iCMC
766 activity to total large iCMC activity in each region for the time period August 2007-July 2012.
767
768 **Figure 11.** (a) Hovmoller diagram of large magnitude (>100 C km) iCMCs for the time period of
769 18-22 June 2011, averaged over latitudes 30°N to 48°N, and spanning longitudes 108°W to
770 78°W. Estimated phase speeds are shown by the dashed red lines and maxima in iCMC activity
771 are shown with red vertical lines. (b) Same as in a), but for sprite-class magnitude (>300 C km)
772 iCMCs. Longitudes of selected 100 C km maxima are shown with black vertical lines, for
773 comparison.
774
775

Tables

Table 1. Tabulation of total iCMC and NLDN CG statistics in each region for the time period August 2007-July 2012.

Region	Large iCMCs > 100 C km			Sprite Class iCMCs >300 C km			NLDN CGs		
	Total	Positive	Negative	Total	Positive	Negative	Total CGs	+CGs	-CGs
PAC	946	813	133	143	140	3	267896	53099	214797
MTN	57907	33625	24282	5132	4669	463	10691221	1050164	9641057
SGP	102130	59462	42668	12623	10598	2025	18266804	2873981	15392823
NGP	257094	213858	42236	27129	25316	1813	16414208	3971396	12442812
LAKE	65159	45400	19759	6568	5938	630	12506941	1672289	10834652
SEUS	322935	143254	179681	26962	20376	6586	48746085	6717658	42028427
NE	4206	3100	1106	395	352	43	1833198	216548	1616650
ATL	137804	54982	82822	8316	5533	2783	16804163	2027868	14776295

Figures

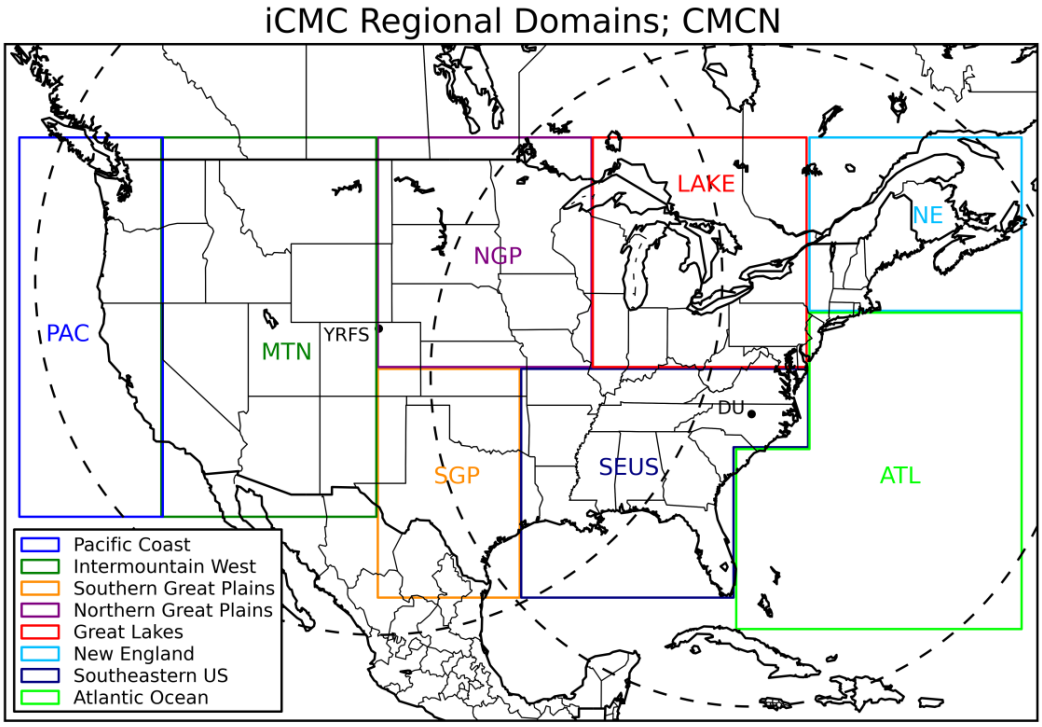

Figure 1. Regional domains used in the analysis of iCMC and NLDN diurnal and seasonal climatologies. The short descriptors are as follows: Southern Great Plains (SGP), Northern Great Plains (NGP), Southeastern US (SEUS), Great Lakes (LAKE), New England (NE), Atlantic Ocean (ATL), Intermountain West (MTN), and Pacific Coast (PAC). Also shown on the map is the coverage of the CMCN (dashed black line) as well as the location of the CMCN sensors at YRFS and DU (black dots).

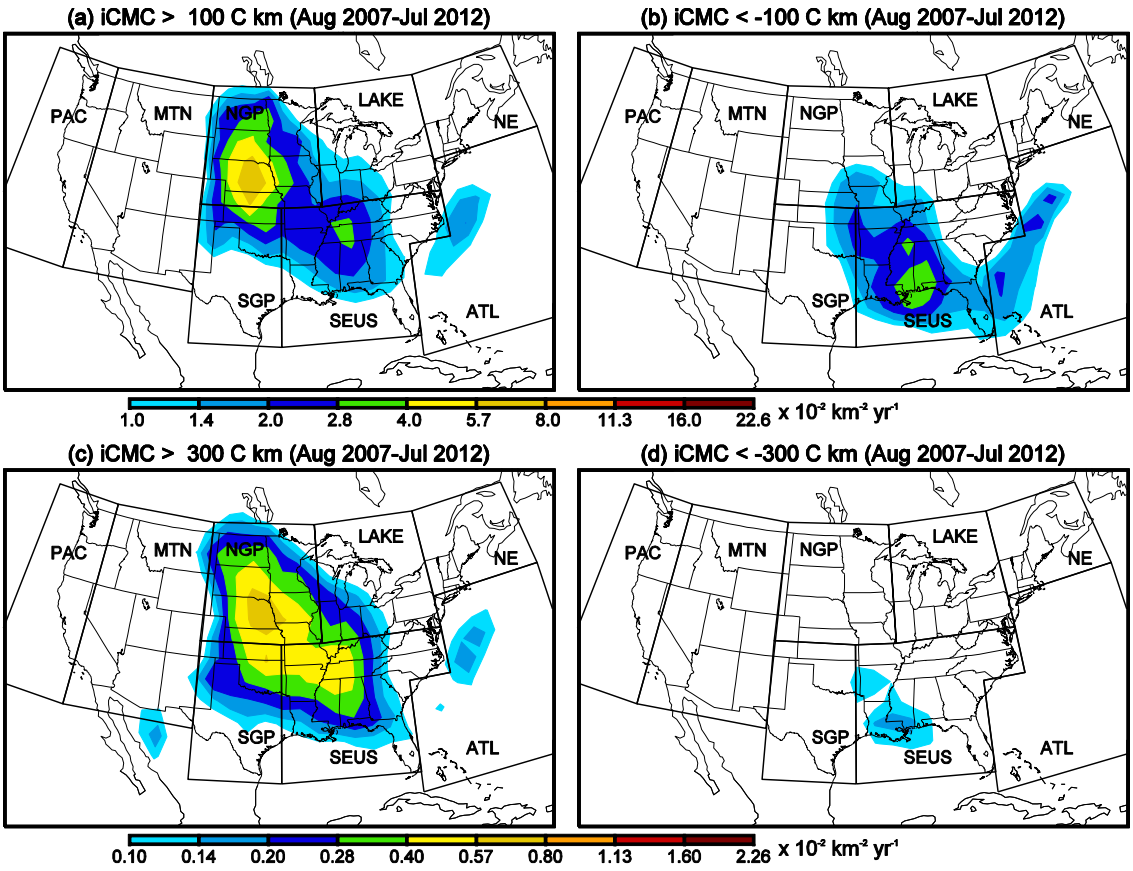

792

793 **Figure 2.** Density maps for strokes with iCMC values greater than 100 C km, for August 2007
794 through July 2012. (a) Positive strokes. (b) Negative strokes; Density maps for strokes with
795 iCMC values greater than 300 C km, for August 2007 through July 2012. (c) Positive strokes. (d)
796 Negative strokes. Note that the two bottom panels for the >300 C km maps are multiplied by 0.1
797 of the scale for >100 C km strokes.

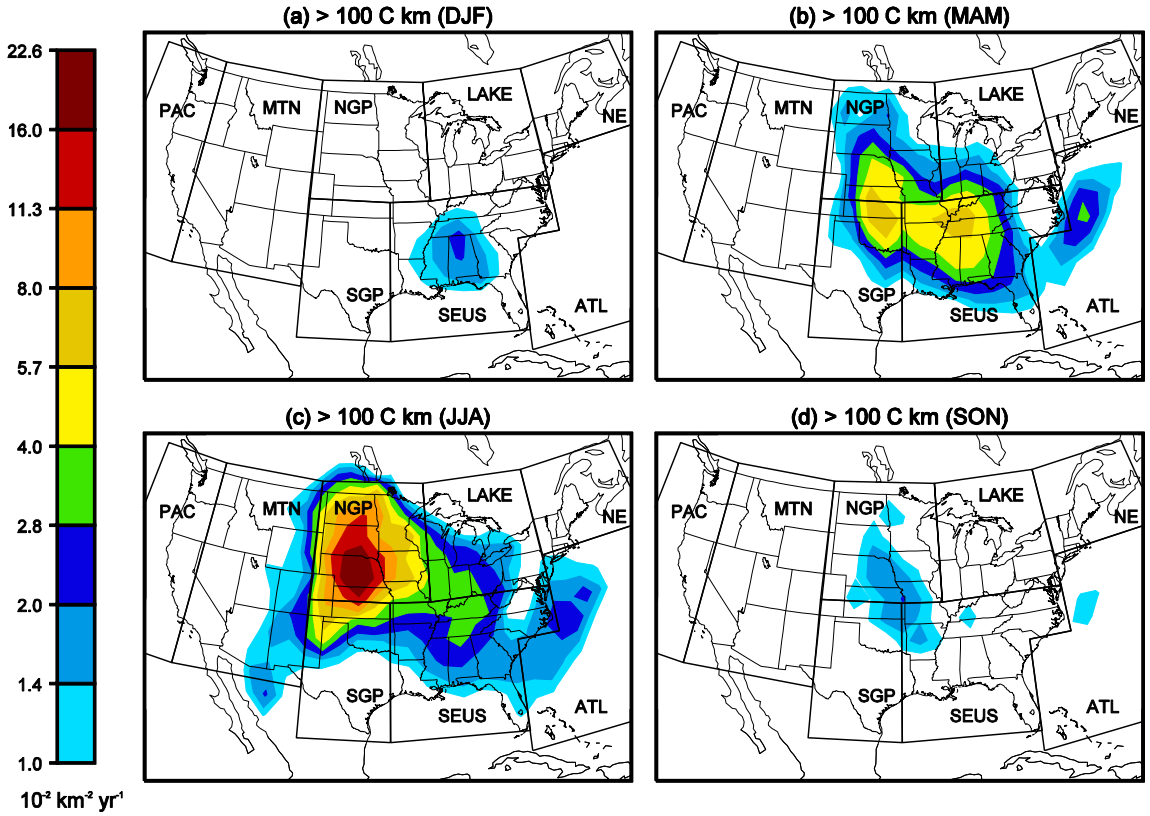

798

799 **Figure 3.** Annualized density maps for positive strokes with iCMC values greater than 100 C km,
800 broken down by season for the period August 2007 through July 2012. (a) December through
801 February (Winter). (b) March through May (Spring). (c) June through August (Summer). (d)
802 September through November (Fall).

803

804

805

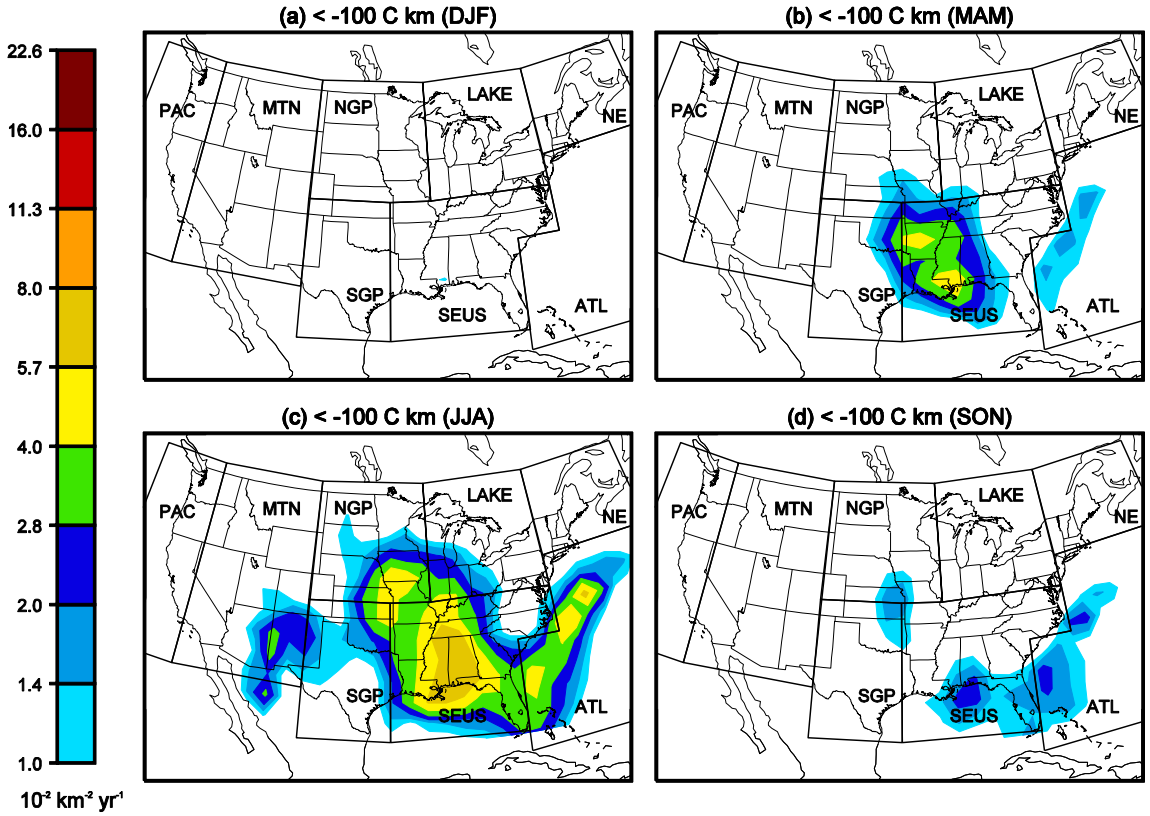

806

807 **Figure 4.** Annualized density maps for negative strokes with iCMC values less than -100 C km,
808 broken down by season for the period August 2007 through July 2012. (a) December through
809 February (Winter). (b) March through May (Spring). (c) June through August (Summer). (d)
810 September through November (Fall).

811

812

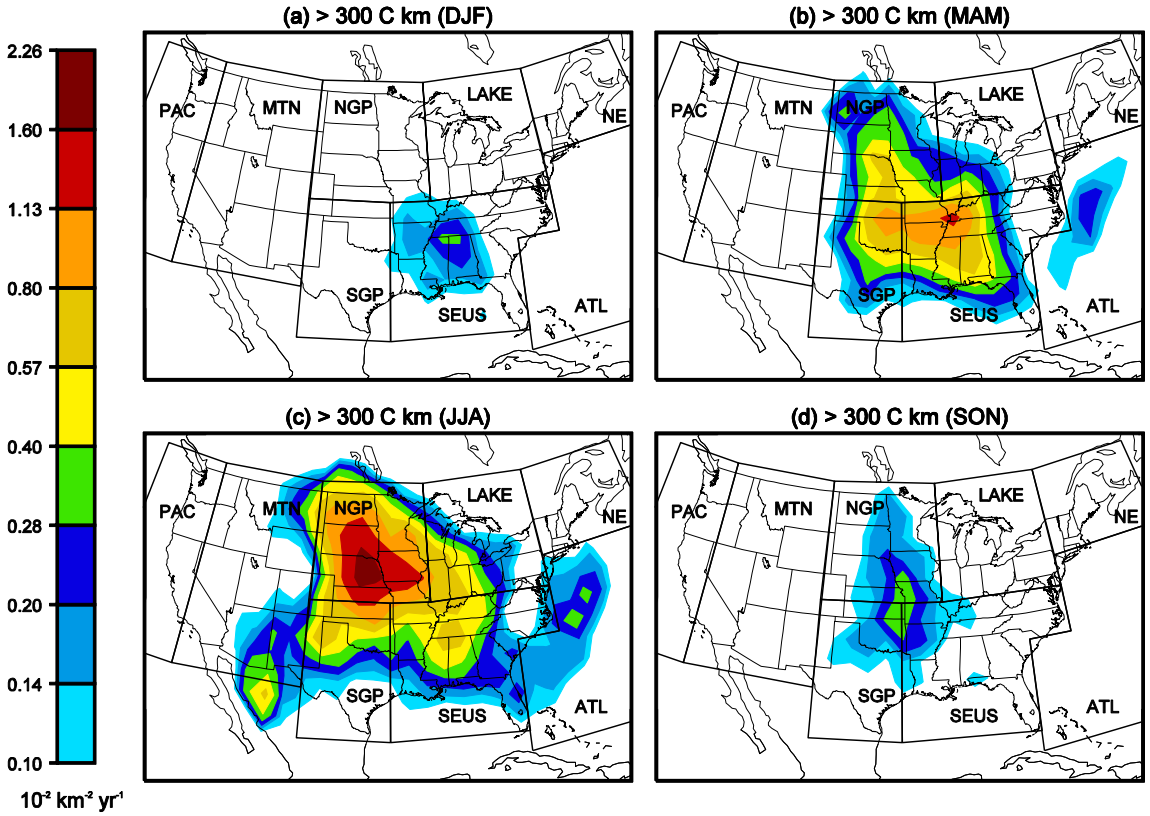

813

814 **Figure 5.** Annualized density maps for positive strokes with iCMC values greater than 300 C km,
815 broken down by season for the period August 2007 through July 2012. (a) December through
816 February (Winter). (b) March through May (Spring). (c) June through August (Summer). (d)
817 September through November (Fall).

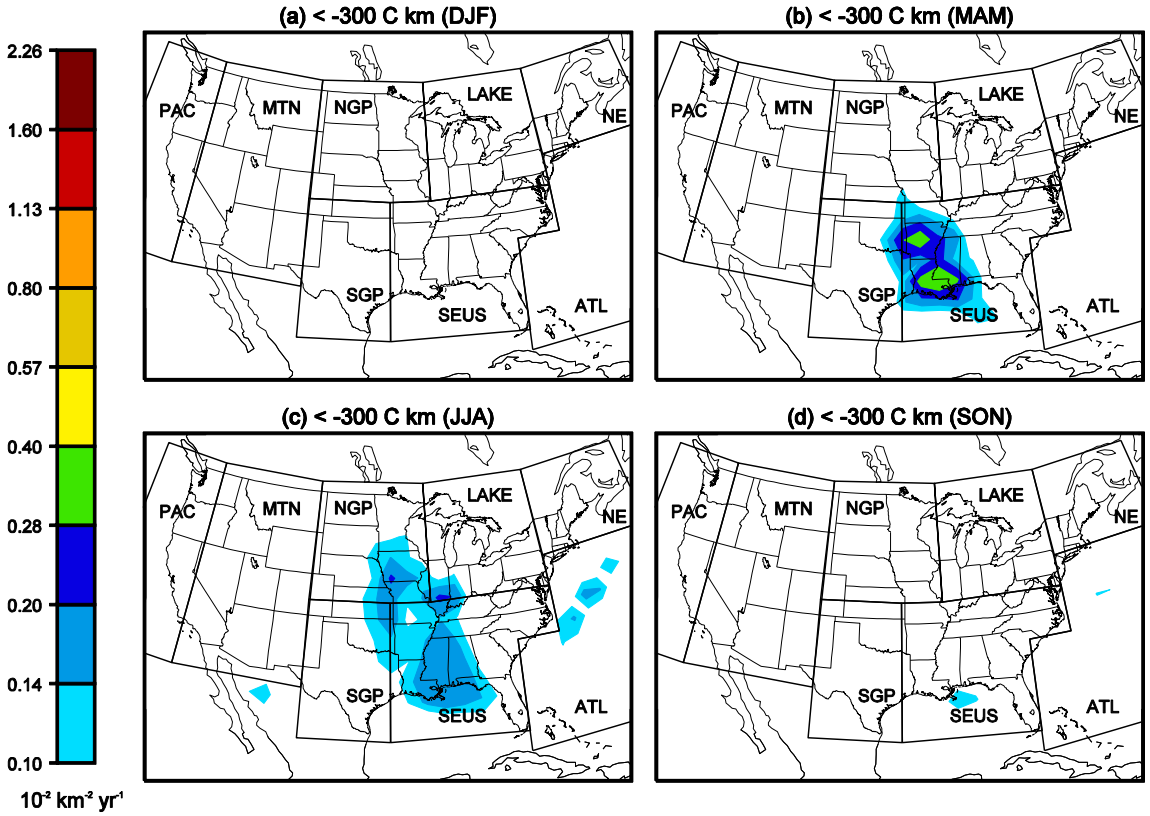

818

819 **Figure 6.** Annualized density maps for negative strokes with iCMC values less than -300 C km,

820 broken down by season for the period August 2007 through July 2012. (a) December through

821 February (Winter). (b) March through May (Spring). (c) June through August (Summer). (d)

822 September through November (Fall).

823

824

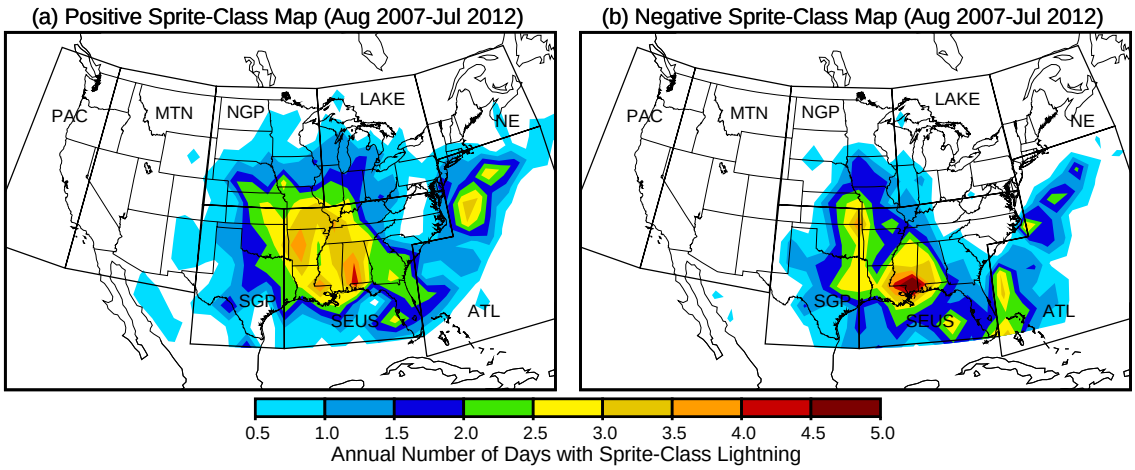

825

826 **Figure 7.** (a) Annual number of days per grid cell with at least one positive sprite-class lightning
827 (iCMC > 300 C km). (b) Annual number of days per grid cell with at least one negative sprite-
828 class lightning (iCMC < -300 C km).

829

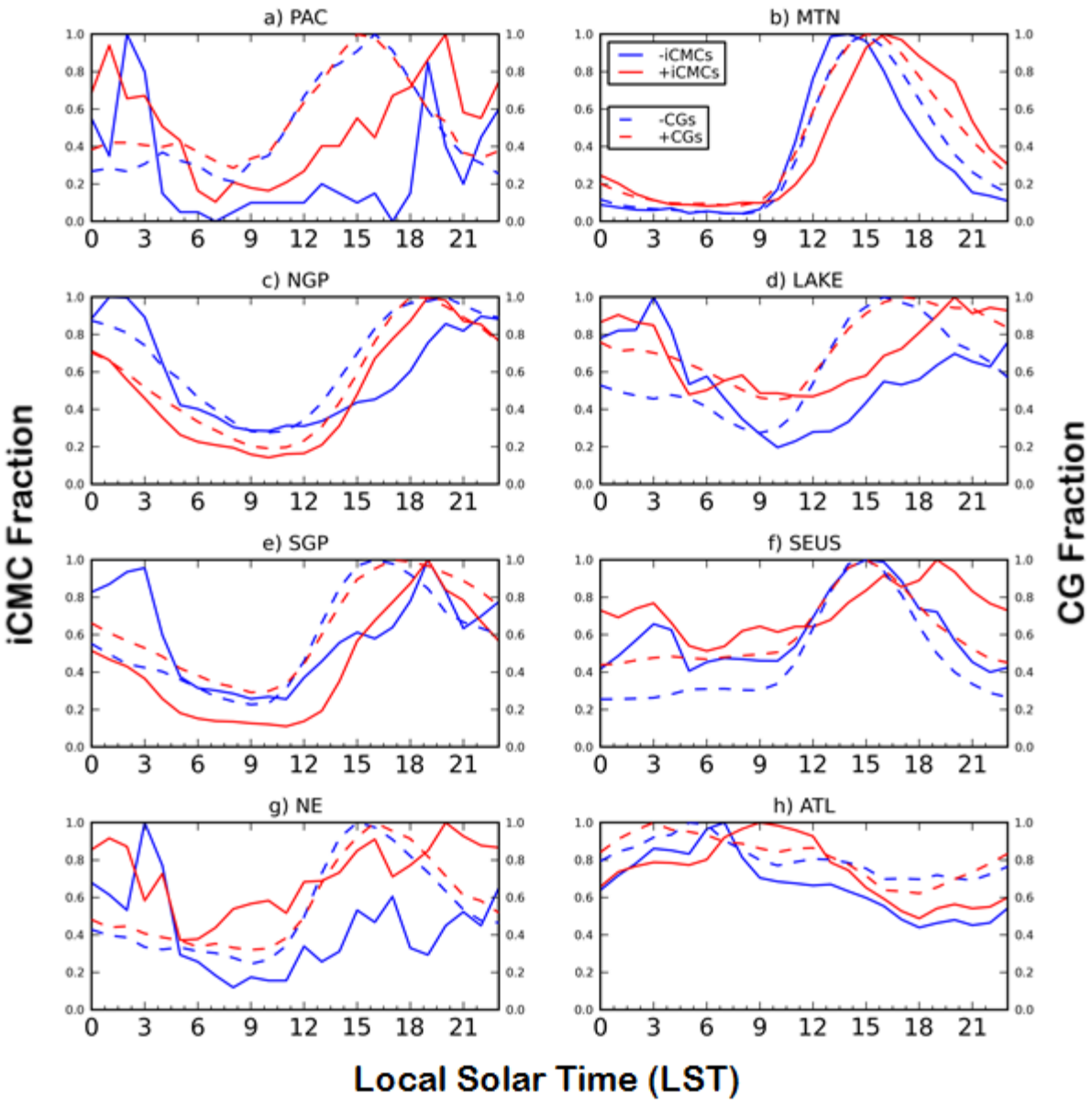

830

831 **Figure 8.** Normalized diurnal distributions of regional iCMC events greater than 100 C km and
832 CG flashes, for the period August 2007- December 2012. (a) Pacific Coast (PAC). (b)
833 Intermountain West (MTN). (c) Northern Great Plains (NGP). (d) Great Lakes (LAKE). (e)
834 Southern Great Plains (SGP). (f) Southeastern United States (SEUS). (g) New England (NE).
835 (h) Atlantic Ocean (ATL).

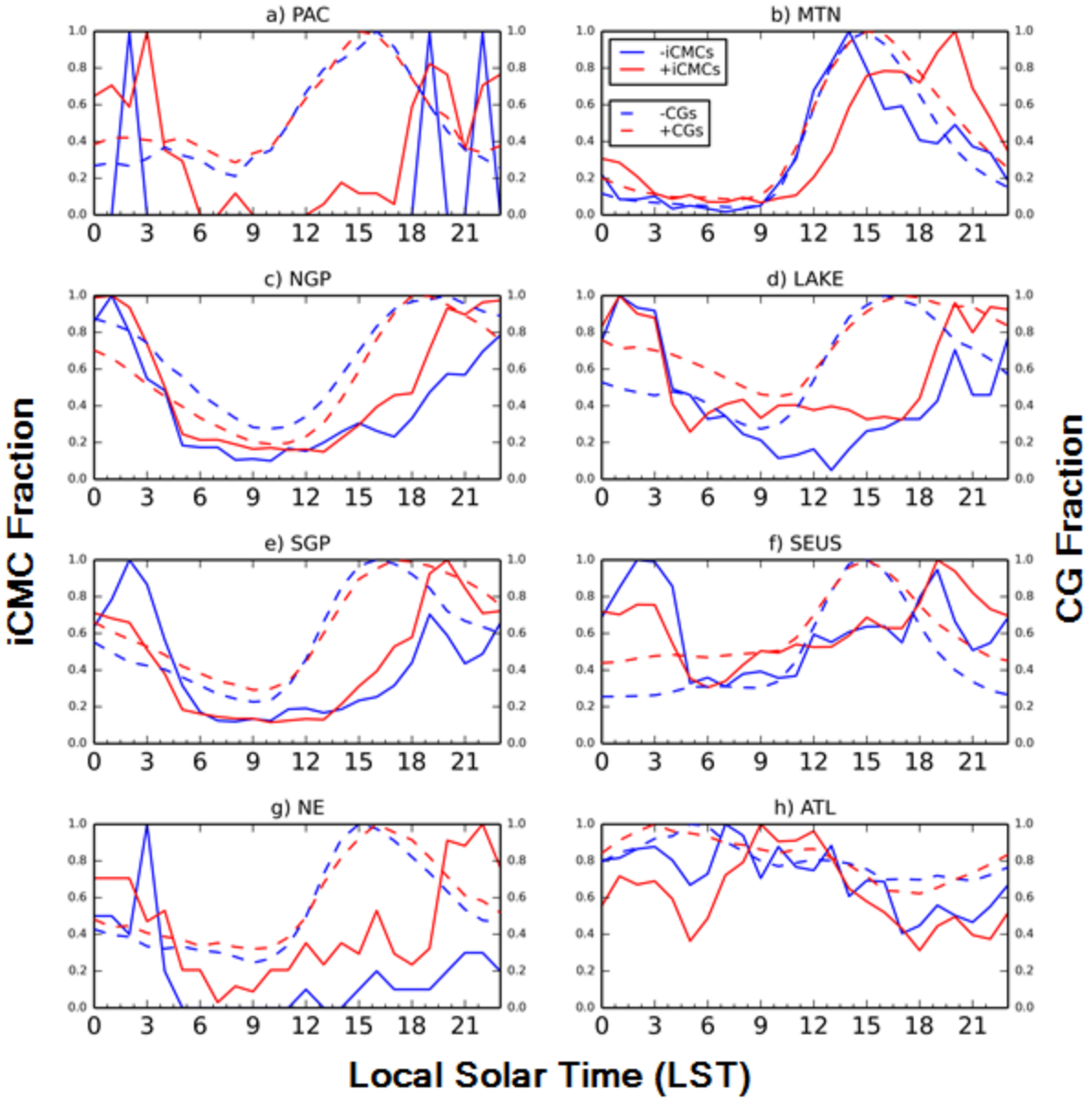

836

837 **Figure 9.** Same as in Fig. 8, but for iCMC events greater than 300 C km.

838

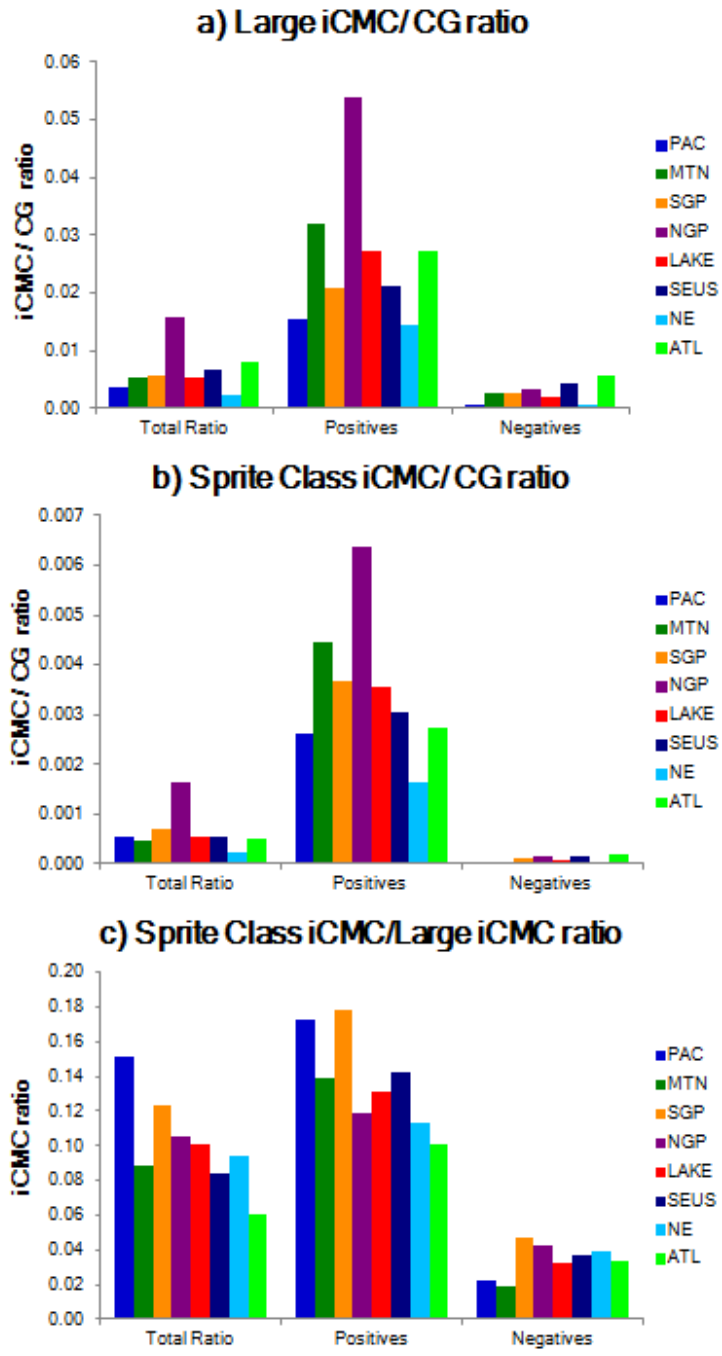

839

840

841 **Figure 10.** Ratios of (a) total large iCMC (>100 C km) activity to total NLDN CG activity, (b) total

842 sprite-class (>300 C km) iCMC activity to total NLDN CG activity, (c) total sprite-class iCMC

843 activity to total large iCMC activity in each region for the time period August 2007-July 2012.

844

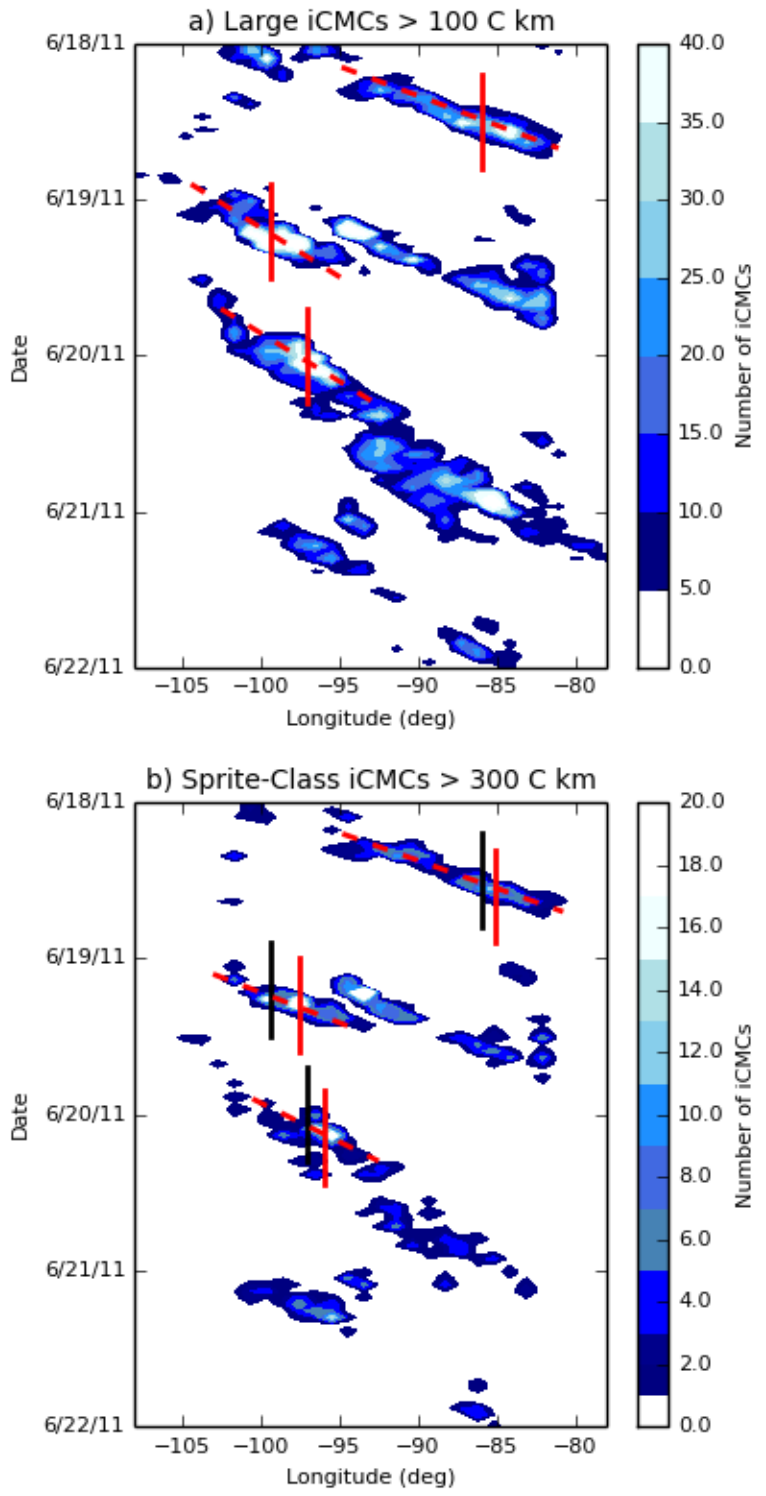

845

846 **Figure 11.** (a) Hovmoller diagram of large magnitude (>100 C km) iCMCs for the time period of

847 18-22 June 2011, averaged over latitudes 30°N to 48°N, and spanning longitudes 108°W to

848 78°W. Estimated phase speeds are shown by the dashed red lines and maxima in iCMC activity
849 are shown with red vertical lines. (b) Same as in a), but for sprite-class magnitude (>300 C km)
850 iCMCs. Longitudes of selected 100 C km maxima are shown with black vertical lines, for
851 comparison.
852